Supplementary Information (SI) for ChemComm.
This journal is © The Royal Society of Chemistry 2026

Supporting Information

Dimensional Engineering of 3D Hierarchical Camellia-like Supramolecular Organic Frameworks for Enhanced Electrochemiluminescence

Kehui Wei,[a] Mingxuan Jia,[a] Huadong Heng,[a] Tianshuo Wang,[b] Lianxi Pu,[b] Yinmin Min,[b] Lijun Ding,[a] Jin Shen[c] and Kun Wang[a,b]*

[a]*School of Agricultural Engineering, Jiangsu University, Zhenjiang 212013, PR China.*

[b]*School of Chemistry and Chemical Engineering, Jiangsu University, Zhenjiang 212013, PR China*

[c]*School of Teacher Education, Jiangsu University, Zhenjiang 212013, PR China*

**Corresponding author*

E-mail address: *wangkun@ujs.edu.cn (K. Wang)*

Contents

1. Experimental section

1.1. Materials and reagents

Potassium peroxodisulfate ($K_2S_2O_8$), Melamine (MA), potassium ferricyanide ($K_3[Fe(CN)_6]$), tetrapotassium hexacyanoferrate trihydrate ($K_4[Fe(CN)_6]$), ethylene diamine tetraacetic acid (EDTA), Tris (hydroxymethyl) aminomethan (Tris), sodium dihydrogen phosphate dihydrate ($NaH_2PO_4 \cdot 2H_2O$), disodium hydrogen phosphate dodecahydrate ($Na_2HPO_4 \cdot 12H_2O$) and ethanol were purchased from Sinopharm Chemical Reagent Co., Ltd. (China). Cyanuric acid (CA) was obtained from Aladdin (China). Potassium chloride (KCl), N-methyl pyrrolidone and dimethyl sulfoxide (DMSO) were purchased from Shanghai Macklin Biochemical Technology Co., Ltd. (China).

Phosphate-buffered saline (PBS, pH 7.4, 0.1 M) was used for all electrochemistry measurements as the supporting electrolyte. Freshly prepared TE buffer (pH 8.0, 10 mM Tris-HCl buffer + 1.0 mM EDTA) was used as aptamer stock solutions. Other HPLC purified DNA sequences were obtained from Sangon Biological Company (Shanghai, China), and every sequence used in this work is listed in Table S1. Ultrapure water obtained from a Millipore water purification system (18.25 MΩ cm^{-1}, Milli-Q, Millipore) was used throughout the whole study. All chemical reagents were received without any further purification.

1.2. Apparatus

The morphology and structure of materials were characterized by transmission electron microscope (TEM, JEOL 2100, Japan) with an acceleration voltage of 200 kV, and scanning electron microscopy (SEM, JSM-7800F, Japan). The X-ray diffraction (XRD) measurements were carried out on diffractometer (Bruker D8, Germany) with Cu kα radiation. And the surface element information was obtained by X-ray photoelectron spectroscopy (XPS, Thermo Fisher Scientific ESCALab QXi, USA). Agarose gel electrophoresis (AGE) was performed using a DYY-6C electrophoresis analyzer (Liuyi, China). All ECL experiments were performed on a model MPI-A electro-chemiluminescence analyzer (Xi'an Remex Analysis Instrument Co. Ltd.

Xi'an, China) with a photomultiplier tube (PMT) biased at 650 V with the range of voltage between -2 to 0 V. Cyclic voltammograms (CVs) and electrochemical impedance spectra (EIS) were conducted using Chenhua CHI-660B electrochemical workstation in 0.1 M KCl solution containing 5 mM $Fe(CN)_6^{3-/4-}$.

1.3. Materials preparation

The 2D material MCA was fabricated employing the procedure described in our prior work.[1]

The 3D camellia-shaped supramolecular organic framework was synthesized according to the literature with certain modifications.[2] In a typical procedure, 1.26 g (0.01 mol) of melamine was dissolved in 80 mL of a dimethyl sulfoxide/N-methyl-2-pyrrolidone mixture (v/v, 9:1) under sonication to obtain solution A. Separately, 1.29 g (0.01 mol) of cyanuric acid was dissolved in 20 mL of the same solvent mixture under sonication to yield solution B. Subsequently, solution A was introduced into solution B, and the mixture was allowed to react at 30 °C for a duration of 5 minutes. The obtained supramolecular product was gathered via centrifugation, rinsed, and then was vacuum-dried. After grinding, a white powder product, denoted as CSOF, was obtained.

1.4. Principles of biosensor design

The toehold-mediated strand displacement (TMSD) strategy has emerged as a powerful and versatile tool in the construction of DNA-based biosensors, primarily owing to its high programmability, rapid reaction kinetics, and isothermal operation without the need for protein enzymes. One of its most compelling advantages lies in the exquisite sequence specificity conferred by the toehold domain, which enables the discrimination of single-nucleotide variations and minimizes false-positive signals in complex biological matrices. Moreover, TMSD inherently supports signal amplification through autonomous target recycling, where each target molecule can participate in multiple displacement events, thereby converting a single binding event into a substantially amplified output. This mechanism not only enhances detection sensitivity but also reduces assay time and operational complexity. In this work, we rationally designed a TMSD-mediated dual-cycle amplification strategy for the

ultrasensitive ECL detection of the aflatoxin-synthesis gene *afl*D. By integrating target-triggered primary displacement with fuel strand-assisted secondary displacement, the system enables repeated release of ferrocene-labeled output strands, leading to a pronounced ECL signal recovery. The following section details the operating principle of this TMSD-based sensing platform.

Initially, a DNA duplex (named as W, constructed by annealing an assistant probe (blue strand, A), an output strand (orange strand, O), and a template strand (green strand, T)) was anchored onto the electrode interface. The ferrocene moiety modified on the output strand quenches the ECL signal of the system. Upon addition of the *afl*D gene, it bound to the first toehold domain of the electrode-bound DNA duplex probe, initiating the first TMSD reaction (TMSD 1). This step displaced and exposed the middle segment of the template strand, which could then hybridize with the fuel strand (purple strand, F) to trigger the second TMSD reaction (TMSD 2). During TMSD 2, the output strand and the *afl*D gene were displaced by the fuel strand. The *afl*D gene was subsequently released and could again hybridize with the template strand, establishing a continuous recycling process. Following repeated cycles, plentiful ferrocene-modified DNA fragments were disengaged from the modified electrode, which reactivated the ECL signal and facilitated ultrasensitive analysis of the aflatoxin-synthesis gene *afl*D.

1.5. ECL measurement procedure

Before modifying the electrode, a glassy carbon electrode (GCE, diameter = 3 mm) was smoothed to a reflective surface using alumina slurries of 0.3 μm and 0.05 μm, and subsequently ultrasonicated in ethanol and deionized water. Subsequently, 10 μL (1.5 mg/mL) of the CSOF dispersion was drop-coated on the prepared GCE, with the solvent then allowed to dry naturally, forming a uniform layer. The DNA duplex was prepared by mixing the template strand, assistant probe, and output strand (12 μM, 100 μL each), followed by a standard thermal cycle. This cycle involved heating to 95 °C and then a controlled ramp-down to 25 °C to facilitate strand hybridization. Then, 10 μL of the resulting DNA duplex solution was dropped onto the CSOF-modified electrode surface

and incubated for 1.5 hours. Afterward, the electrode was rinsed with 1× TE buffer to remove unbound residues. The modified electrode was then immersed in a hybridization solution containing the Fuel strand and target DNA at varying concentrations. Finally, the assembled biosensor was placed into 0.1 M PBS (pH 7.4, 10 mL) enriched with 50 mM $S_2O_8^{2-}$. The ECL measurement was conducted within a potential window from -2 V to 0 V at a sweep speed of 100 mV/s. The PMT bias voltage and the amplifier gain were set to 650 V and 3, respectively.

1.6. Agarose gel electrophoresis analysis

Agarose gel (1.8 g) was dissolved in 1× TE buffer by microwave heating until complete dissolution yielded a clear solution. Subsequently, 5 μL of the red nucleic acid stain ethidium bromide (EB) was added to the solution and mixed thoroughly. The mixture was poured into a gel casting tray. After the gel solidified completely, the comb was detached with care, and the gel slab was then positioned in an electrophoresis chamber filled with 1× TE buffer. For sample loading, 10 μL of the sample was combined with 2 μL of loading buffer. A 5 μL aliquot of the resultant mixture was then carefully pipetted into the sample wells. Electrophoresis was performed at a constant voltage of 120 V until the dye front migrated approximately three-quarters of the gel length. The gel was then removed and the DNA bands were visualized under UV illumination.

1.7. LOD calculation

According to the definition adopted by the International Union of Pure and Applied Chemistry (IUPAC), the LOD is determined by the lowest signal value (x_L) that can be detected with reasonable certainty for a given analytical procedure. The value of x_L is given by the equation: $x_L = \bar{x_b} + k*SD$ (where $\bar{x_b}$ is the mean of the blank, SD is the standard deviation of the blank, k is a numerical factor selected according to the confidence level). In this study, the $\bar{x_b}$ as measured for LOD calculation is 518.1 a.u., and the corresponding SD is 1.85. Normally, the value of k is set as 3 corresponding to a confidence level of 99.1%.[3]

According to the linear regression equation: $I_{ECL} = 1384.28 \lg C + 7473.86$, the LOD

was calculated as 9.5 fM.

1.8. Calculation of entropy increase

To confirm the core efficacy of the entropy-driven signal amplification system, the corresponding thermodynamic principles were applied to determine the Gibbs free energy change depicted in Figure S8G.

$$\Delta G = \Delta H - T\Delta S \qquad (1)$$

Equation 1 denotes the parameters ΔH, ΔS, and T as the enthalpy change, entropy change, and thermodynamic temperature of the system, respectively. Under the condition that the base pair count is invariant during the reaction, $\Delta H \approx 0$. It follows that the reaction proceeds due to a thermodynamic drive stemming from the entropy gain of released molecules, with this driving force invariably given by TΔS.[4]

Consequently, the final concentration of each component can be determined on the basis of the Gibbs free energy change defined in Equation (2).

$$\Delta G = \Delta G_P^0 + \Delta G_A^0 + \Delta G_O^0 - \Delta G_W^0 - \Delta G_F^0 + RT\ln Q \qquad (2)$$

Herein, Q and ΔG_x^0 are termed as reaction quotient and free energy of corresponding species in standard conditions, respectively. R represents the gas constant (8.314J/mol •K). They are described by Tris-HCl buffer solution with the condition of 0.1 mol L^{-1} Na^+, 0.05 mol L^{-1} Mg^{2+}, 25 °C, and c^0 = 1 mol L^{-1}. The parameter Q can be represented by equation (3).

$$Q = \frac{([P]/c^0)([A]/c^0)([O]/c^0)}{([W]/c^0)([F]/c^0)} \qquad (3)$$

While ΔG0 X can be obtained with assistance of NUPACK software, and expressed in equation (4).

$$\Delta G_P^0 + \Delta G_A^0 + \Delta G_O^0 - \Delta G_W^0 - \Delta G_F^0 = 1.63 \text{ kcal/mol} \qquad (4)$$

Then, Q value of 0.0639 can be calculated in the condition of reaction in equilibrium according to equations (2) and (4), where ΔG = 0.

According to Figure S7, the initial concentrations of both W and F are 100 nmol L^{-1} and the final concentration of P is x nmol L^{-1}. Then the following equation can be given

according to the equation (3).

$$\frac{\left(10^{-9}x\right)^3}{\left[10^{-9}(100 - x)\right]^2} = 0.0639$$

The value of x can be estimated to be between 99 and 99.9 nM through the bisection method, indicating that the system can theoretically convert 99% of the reactant substrate into the product.[5]

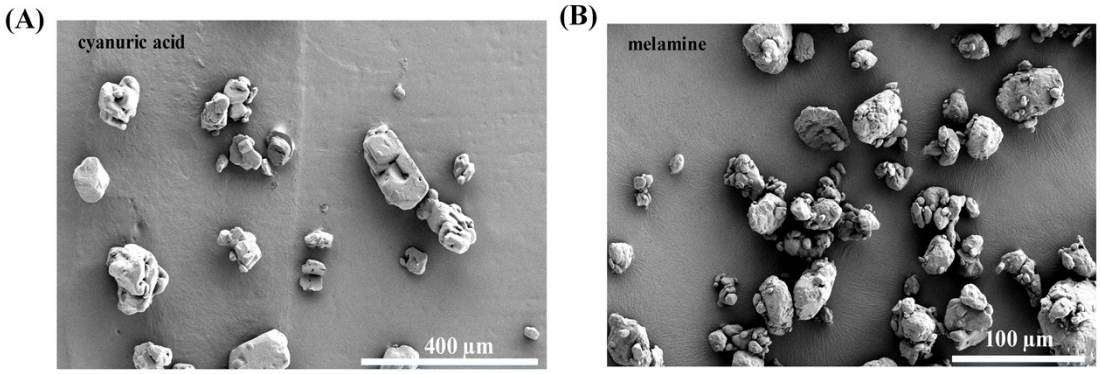

Figure S1. SEM images of (A) cyanuric acid and (B) melamine.

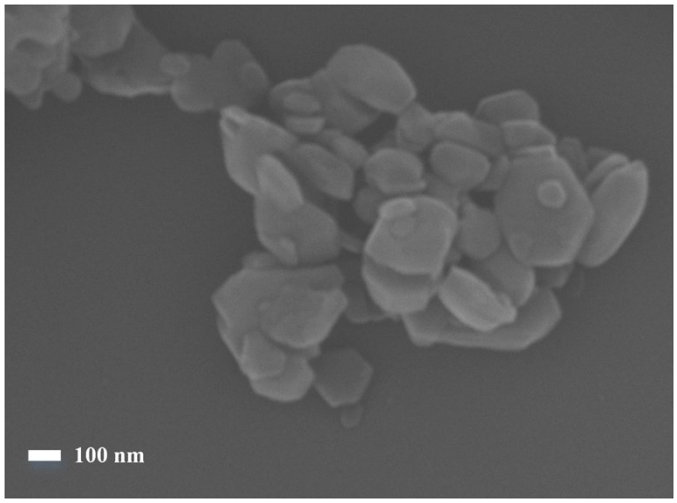

Figure S2. SEM image of MCA.

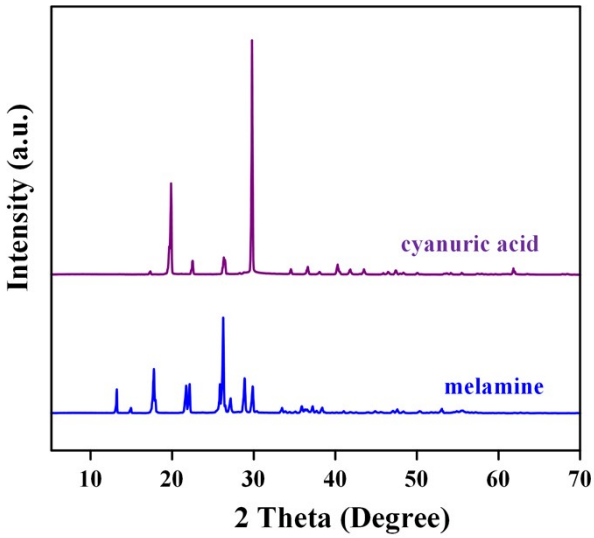

Figure S3. XRD profiles of cyanuric acid and melamine.

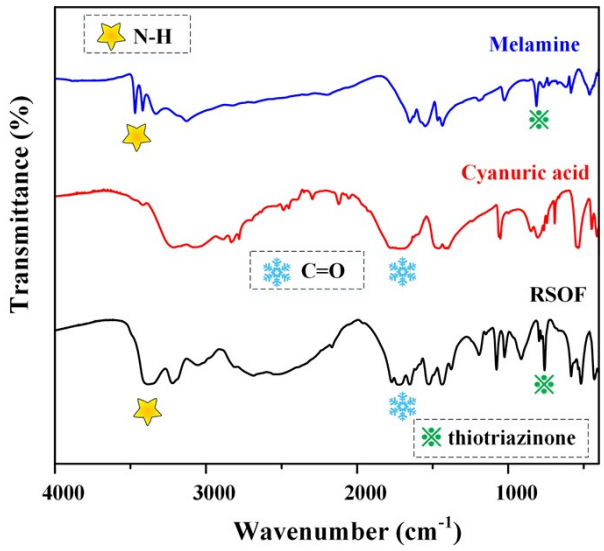

Figure S4. FT-IR spectra of melamine, cyanuric acid and CSOF.

Notes: As shown, the C=O stretching vibration of cyanuric acid shifted from 1716 cm^{-1} to a higher wavenumber at 1736 cm^{-1}, while the triazine ring stretching vibration of melamine shifts from 812 cm^{-1} to a lower wavenumber at 759 cm^{-1}. The downshift of the triazine ring vibration in melamine and the upshift of the C=O stretching vibration in cyanuric acid indicate the formation of intermolecular hydrogen bonds, specifically N-H···O and N-H···N interactions between adjacent molecules. These results provide clear evidence for the successful formation of the synthesized nanomaterial.

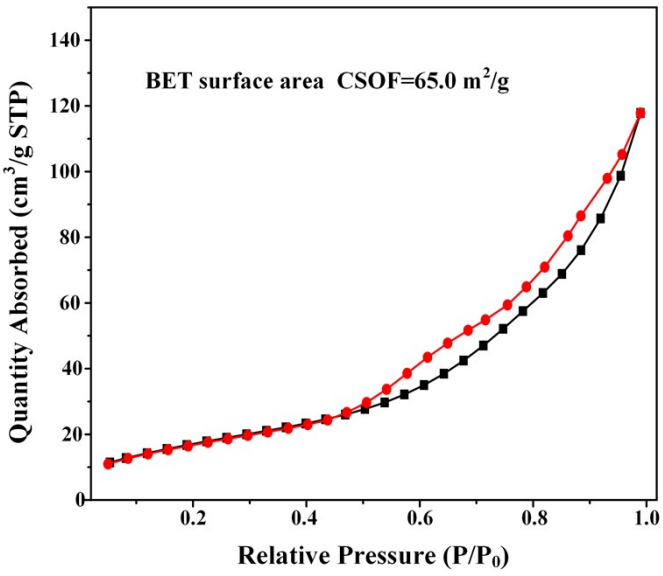

Figure S5. N_2 adsorption-desorption curves of CSOF.

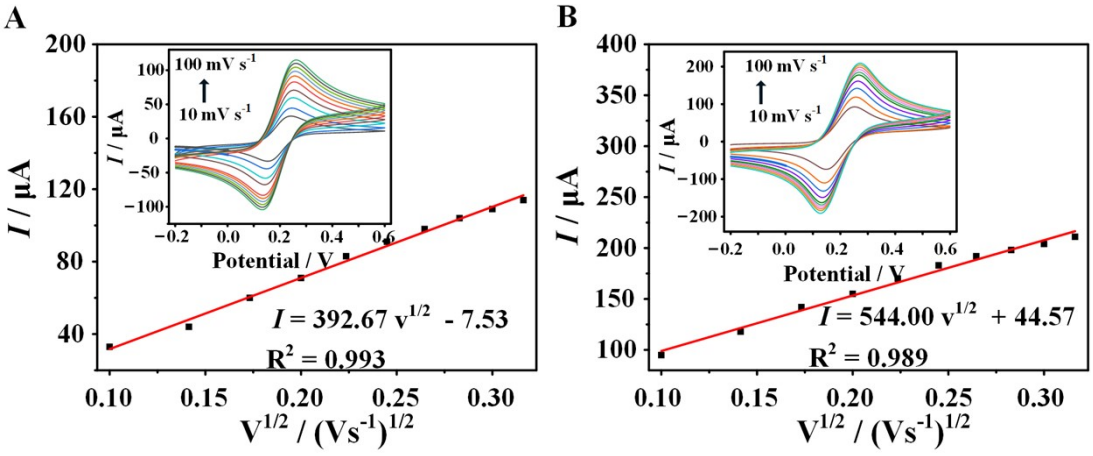

Figure S6. CV curves and linear relations of electrodes modified with (A) MCA and (B) CSOF in 5.0 mmol/L of $[Fe(CN)_6]^{4-/3-}$ in scan rates range of 10-100 mV s^{-1}.

Notes: The electrochemical active surface areas of CSOF and MCA were determined via cyclic voltammetry (CV) based on the Randles-Sovcik equation:[6]

$$I = 2.69 * 10^5 A D^{1/2} n^{3/2} v^{1/2} c$$

The electrochemical active surface area (A, cm^2) was determined from the slope of the linear regression of peak current (I) against the square root of scan rate ($v^{1/2}$). The calculation

employed the following parameters: the number of electrons transferred (n = 1), the diffusion coefficient (D = 6.70 ± 0.02 × 10^{-6} cm^2 s^{-1} at 25 °C), and the concentration of the redox couple ($[Fe(CN)_6]^{4-/3-}$, c = 5 mM).[7]

Based on the dependence of voltammetric peak intensities on the square root of potential sweep rates in the cyclic voltammetry (CV) profiles (Figures 3A-B), with linear fitting equations of $I = 392.67\ v^{1/2} - 7.53$ as well as $I = 544.00\ v^{1/2} + 44.57$, the calculated A for MCA was 0.113 cm^2, which was lower than that of CSOF (0.156 cm^2). This result indicated a significantly enhanced electroactive surface area for CSOF, attributable to the synthesized 3D hierarchical camellia-like superstructure. Furthermore, the increased current response of CSOF compared to MCA suggested an improvement in electron transfer kinetics.[8]

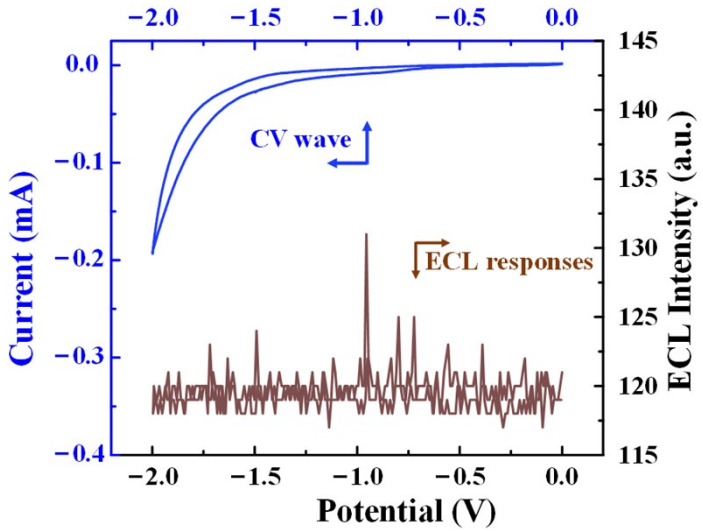

Figure S7. ECL-potential profiles and its corresponding CV curves (blue line) of CSOF in PBS (0.1 M, pH 7.4).

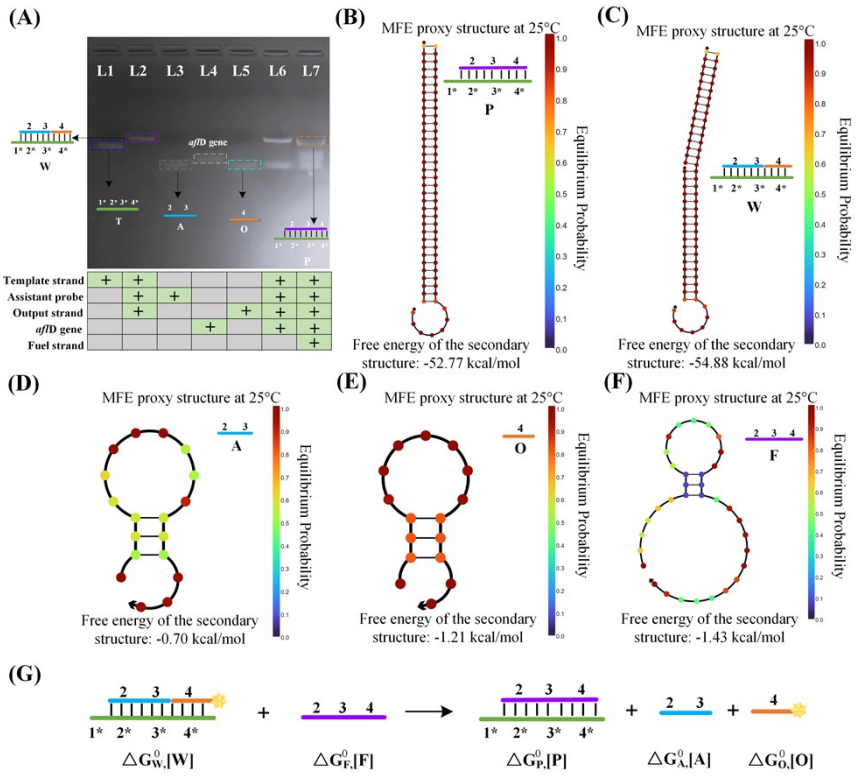

Figure S8. (A) Gel electrophoresis analysis of different samples. Secondary structures and standard free energies of the components in the entropy-driven reaction predicted by NUPACK: (B-F) Strand P, W, A, O and F; (G) Strand displacement reaction equation with thermodynamic parameters.

Notes: The performance of the designed entropy-driven amplifier was evaluated using agarose gel electrophoresis. As presented in Figure S8, lane 1 displayed a distinct band corresponding to the template strand. Subsequently, the assistant probe, output strand, and template strand formed a DNA ternary complex that served as the substrate for the entire entropy-driven system (lane 2). Lanes 3, 4, and 5 represented the assistant probe, *afl*D gene, and output strand, respectively. Samples in lanes 6 and 7 corresponded to W + *afl*D gene, and W + *afl*D gene + fuel strand, respectively. Upon the introduction of the *afl*D gene into the DNA duplex system, a band corresponding to the assistant probe appeared, indicating that the *afl*D gene could hybridize with the DNA duplex probe and displaced the assistant probe (second band in lane 6). When the DNA duplex probe, *afl*D gene, and fuel strand were mixed together (lane 7), the TMSD reaction was triggered. Driven by the hybridization of the *afl*D gene, the assistant probe was released from the DNA duplex (third band in lane 7), while the template strand hybridized with the fuel strand to form a double-stranded DNA product (first band in lane 7). Furthermore, this process resulted in the displacement of the *afl*D gene (second band in lane 7) and the output strand (third band in lane 7) from the original DNA duplex probe. These results collectively validated the feasibility of the TMSD mechanism.

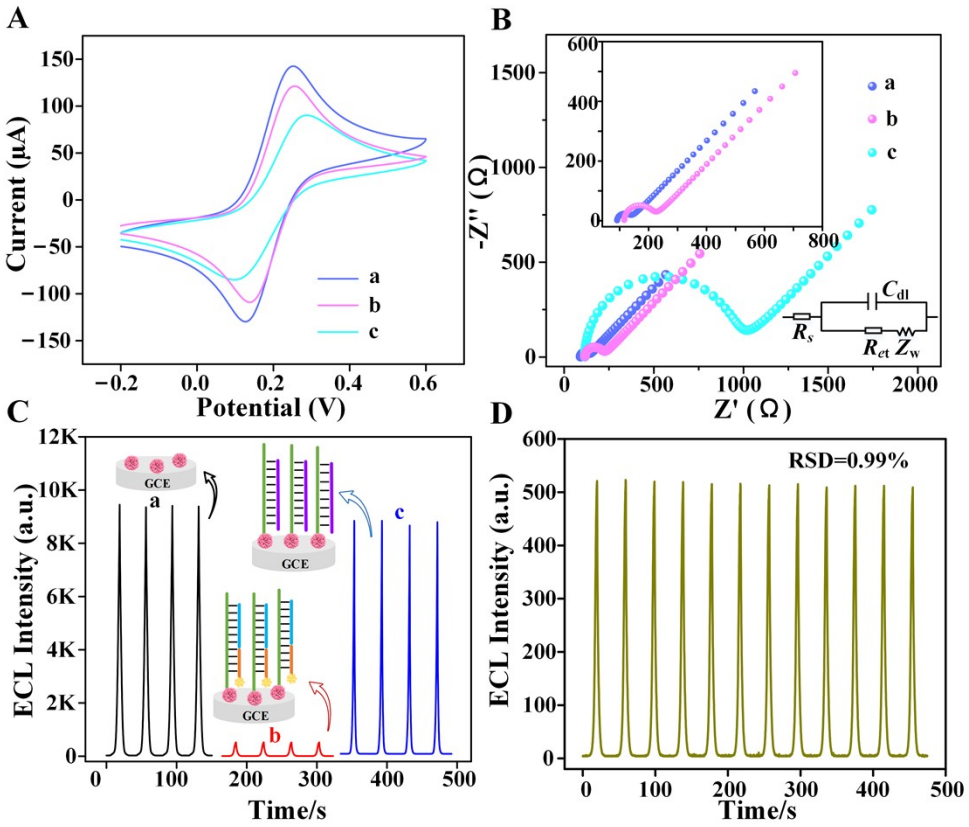

Figure S9. (A) CV curves and (B) EIS plots of different modified electrodes in 0.1 M KCl with 5 mM $[Fe(CN)_6]^{3-/4-}$: (a) bare GCE; (b) CSOF/GCE; (c) DNA duplex/CSOF/GCE; (C) ECL behavior of CSOF/GCE (a), DNA duplex/CSOF/GCE (b), and FT probe/CSOF/GCE in PBS (0.1 M, pH 7.4) with 0.05 M $K_2S_2O_8$ and (D) ECL-time profiles recorded from 12 consecutive cycles of the DNA duplex/CSOF/GCE in the $K_2S_2O_8$ (4 μM, pH 7.4).

Notes: It could be seen that a pair of well-defined redox peaks was observed on the bare GCE (Figure S9A, curve a). When modified with CSOF, the maximum current observed in the cyclic voltammogram (curve b) declined slightly. A significant current attenuation was recorded following the immobilization of the DNA duplex probe onto the electrode (curve c), owing to the electrostatic repulsion between the anionic phosphate groups of DNA and the $[Fe(CN)_6]^{3-/4-}$ couple.[9] Therefore, the rational variation in peak currents in the CV profiles confirms the successful stepwise construction of the biosensor.

As another prevalent technique for probing the stepwise assembly of ECL sensors, EIS offers a direct probe for alterations in interfacial resistance throughout the electrode modification

process.[10] Figure S9B depicted the EIS responses of differently modified electrodes. The impedance spectrum is generally composed of a high-frequency semicircle and a low-frequency linear segment. The semicircular signal found at higher-frequency ranges arose from a charge-transfer-limited mechanism; the diameter of this arc provided a measure of the charge-transfer resistance (R_{et}), serves as a key indicator for modifications occurring at the electrode surface. The low-frequency linear portion represents the diffusion-controlled process.[11] The results showed that the Nyquist plot of the CSOF/GCE exhibited a slightly larger semicircle (R_{et} = 96.51 Ω) compared to the bare GCE (R_{et} = 42.53 Ω), which could be attributed to the thin film on the electrode surface hindering electron transfer. Upon immobilization of the DNA duplex probe onto the CSOF/GCE, a substantial increase in R_{et} was observed (R_{et} = 827.1 Ω). This substantial increase stemmed from electrostatic repulsion between the DNA phosphate groups and the ferricyanide/ferrocyanide couple.[12] These EIS results were consistent with the CV data, jointly verifying the effective assembly of the ECL sensor.

To further validate the on-electrode operation of the TMSD reaction process, ECL measurements were conducted (Figure S9C). The immobilization of CSOF on the GCE surface produced a pronounced increase in ECL intensity (9450 a.u.; curve a), indicating that CSOF serves as an excellent ECL-active material. Upon immobilization of the DNA duplex probe labeled with a ferrocene moiety on CSOF, a markedly attenuated ECL signal was recorded at the DNA duplex/CSOF/GCE electrode, with the intensity quenched to 5.3% (approximately 500 a.u., curve b). The observed quenching is most likely attributable to oxidation of Fc to Fc^+, which markedly perturbs the redox processes that underlie the ECL system.[13] Subsequent addition of a mixture containing the *afl*D gene and the fuel strand triggered a TMSD, displacing the ferrocene-bearing output strand away from the electrode and restoring the ECL signal to near its initial intensity (curve c). These results validate the design concept of the detection platform. Additionally, the reliability of the quenching action was evaluated under uninterrupted repetitive scanning conditions (Figure S9D). Minimal fluctuation was detected in the ECL response (relative standard deviation < 1%), confirming the robustness and reliability of the proposed method.

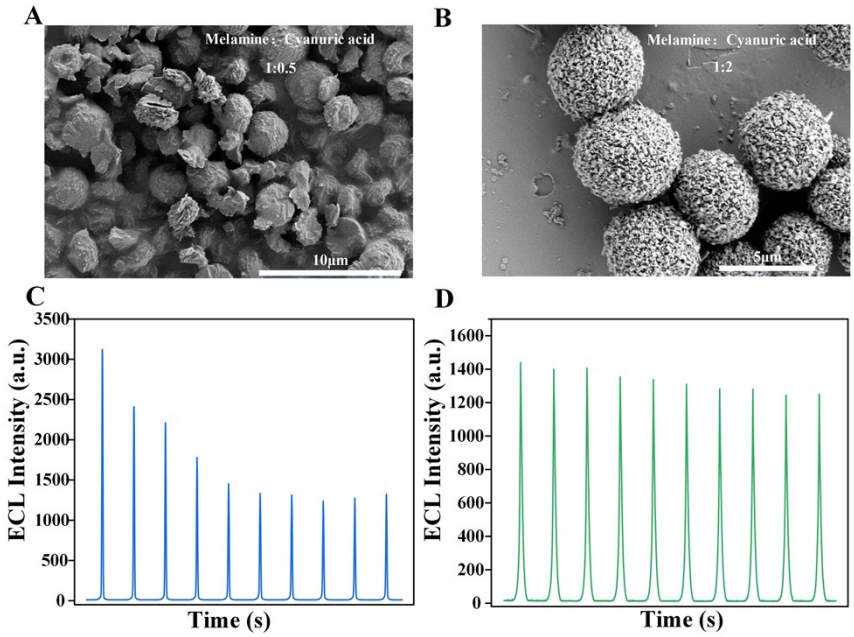

Figure S10. SEM images of (A) CSOF-0.5 and (B) CSOF-2 prepared with different molar ratios of melamine to cyanuric acid; ECL responses of (C) CSOF-0.5 and (D) CSOF-2 in the solution containing 0.1 mol L^{-1} PBS (pH 7.4) and 0.05 mol L^{-1} $K_2S_2O_8$.

Notes: First, with the feed ratio (MA:CA molar ratio, represented by x in the sample designation CSOF-x) varied at 1:0.5, 1:1, and 1:2, its effects on the structural features and ECL performance of the materials were systematically explored. As the MA/CA ratio increased from 1:0.5 to 1:2, the morphology of CSOF evolved sequentially from irregular particles (Figure S10A) to a flower-like hierarchical structure, and finally to a spherical architecture assembled from individual particles (Figure S10B). CSOF-0.5 exhibited a poorly defined structure, which led to hindered electron transfer and structural instability, resulting in relatively poor ECL performance (Figure S10C). Although CSOF-2 displayed a superstructure, its densely packed particle configuration likely restricted reactant diffusion and offered limited active sites for electron transfer and reactions, leading to weak ECL intensity (Figure S10D).[14] In contrast, when the MA/CA feed ratio was 1:1, the material formed a three-dimensional organic superstructure self-assembled from low-dimensional segments. This hierarchical architecture fully exposed active sites and facilitated efficient ion transport, thereby yielding excellent ECL performance. Accordingly, the material synthesized at an MA/CA feed ratio of 1:1 was selected for further study.

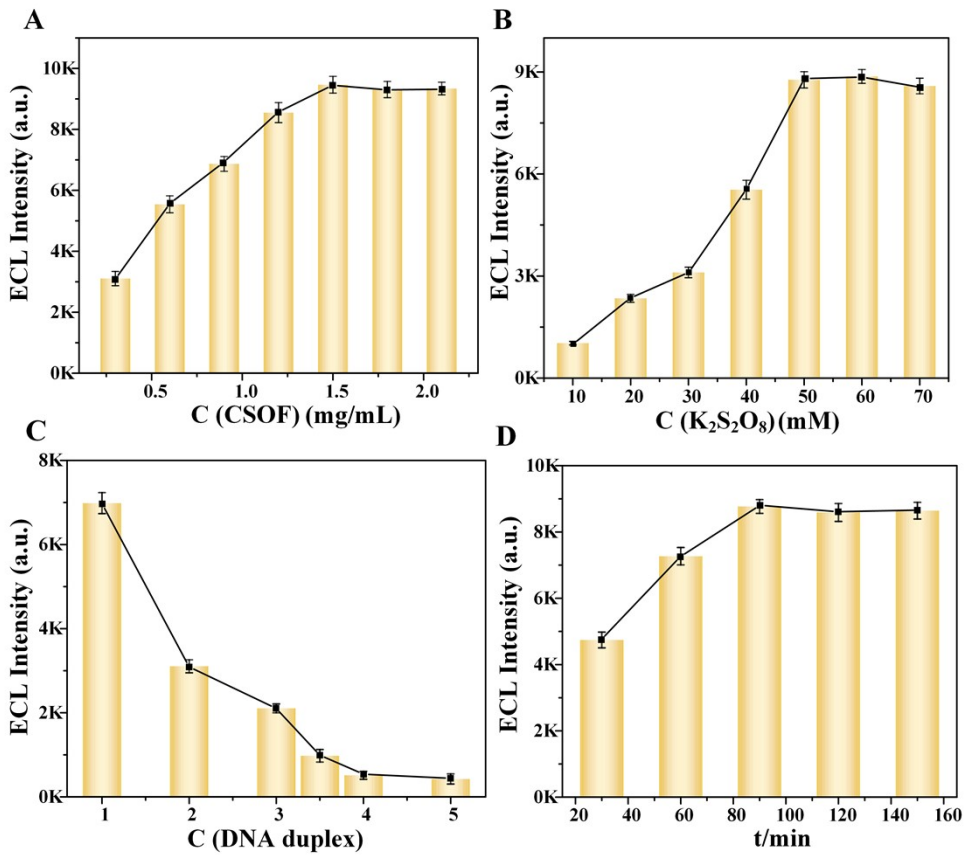

Figure S11. CSOF concentration (A), optimization of the co-reactant $K_2S_2O_8$ concentration (B), DNA duplex probe concentration (C), and the response time of toehold-mediate strand displacement reaction (D).

Notes: Critical parameters affecting sensor performance, including CSOF dosage and $K_2S_2O_8$ concentration, were systematically optimized. We first optimized the CSOF concentration based on ECL intensity (Figure S11A). A maximum signal was achieved at 1.5 mg/mL, establishing this as the optimal dosage. Next, we examined the effect of the co-reactant $K_2S_2O_8$. The ECL intensity peaked at 50 mM and plateaued beyond this point (Figure S11B), suggesting efficient co-reaction dynamics at this concentration. Accordingly, 50 mM was chosen for all further studies. Further optimization was performed on the immobilization concentration of the DNA duplex probe and the TMSD reaction time. According to Figure S11C, a progressive decline in ECL intensity was recorded when the probe concentration was raised from 1 to 4 μM, signaling a marked quenching effect by the ferrocene moiety. A further increase in concentration resulted in no significant additional signal reduction. An immobilization

concentration of 4 μM was therefore selected for subsequent experiments. The impact of incubation time on sensor behavior was then evaluated. ECL signal magnitude grew with incubation from 30 to 90 minutes and thereafter plateaued (Figure S11D), suggesting that the TMSD process had achieved equilibrium after 90 minutes. Hence, an incubation time of 90 minutes was selected as optimal.

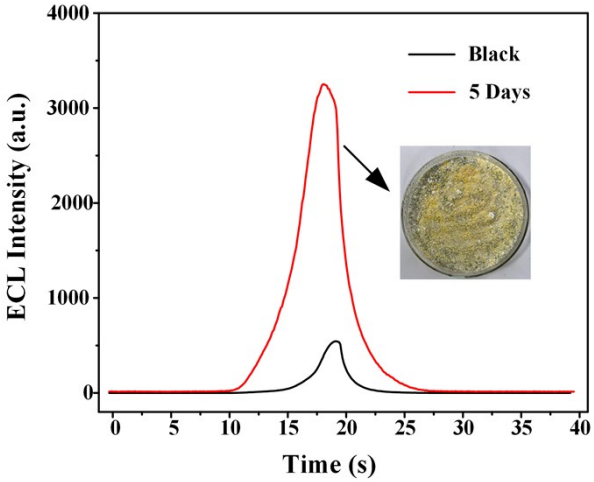

Figure S12. Electrochemiluminescence biosensor response of aflatoxin-positive corn flour after five days of incubation with *Aspergillus flavus*.

Table S1 Sequences of DNA used in the experiment.

Name	Sequence (5'-3')
Template strand (T)	COOH-TTGGAGTTGAGATCCTTAGACTACCAGGGGAGTTGAGATCC
Assistant probe (A)	AACTCCCCTGGTAGTCTA
Output strand (O)	AGGATCTCAACTCCAA-Fc
Fuel strand (F)	AACTCCCCTGGTAGTCTAAGGATCTCAACTCCAA
Target	GGATCTCAACTCCCCTGGTAG
M-8	CCAGCTCATGTCCCAAGGTCG
M-5	GGTTCTGAAATCCCTTGGCAG
M-2	GGATGTCAACTCGCCTGGTAG
Random	TCGTGACTGGGATTCACTAGT

M-8: Eight mismatched bases located at the same position;

M-5: Five mismatched bases located at different positions;

M-2: Two mismatched bases located in two different positions;

Random: Random DNA sequences.

Table S2 Comparison of the sensing performance of available platforms for *afl*D.

Method	Linear range	Detection limit	Reference
Fluorescence detection	0.1nM - 100 nM	12.83pM	15
Fluorescence detection	0.5 nM -500 nM	0.75 nM	16
Fluorescence detection	0.05 nM - 200 nM	0.02 nM	17
Electrochemical biosensor	1 nM - 10 μM	0.55 nM	18
Fluorescence detection	5 pM - 50 nM	1.66 pM	19
Electrochemilumine-scence	0.5 nM - 250 nM	0.4 nM	1
Electrochemilumine-scence	10 fM - 10 nM	9.5 fM	this work

Table S3 Recoveries of *afl*D genes in the corn flour samples (n=3).

Sample	No.	Added (nM)	Found (nM)	Recovery (%)	RSD (%)
Corn flour	1	0.005	0.0049	98.0	1.7
	2	0.05	0.041	82.0	8.3
	3	0.5	0.55	110.0	6.8

References

[1] K.-H. Wei, Q. Liu, M.-X. Jia, H.-D. Heng, L.-J. Ding, J. Shen, M. Zhang, D.-P. Wang and K. Wang, *Chem. Commun.*, 2025, **61**, 16444-16447.

[2] Z. Song, L. Miao, L. Ruhlmann, Y. Lv, L. Li, L. Gan, M. Liu, *Angew. Chem. Int. Ed.*, 2023, **62**, e202219136.

[3] X. Zhong, S.-S. Yang, N. Liao, R. Yuan, Y. Zhuo, *Anal. Chem.*, 2021, **93**, 5301-5308.

[4] Li, H.; Cao, Y.; Wu, T.; Zhang, Y.; Zheng, Z.; Lv, J.; Mao, A.; Zhang, Y.; Tang, Q.; Li, J. *Anal. Chem.,* 2021, **93**, 11043-11051.

[5] Chen, Y.; Xu, L.; Xu, Q.; Wu, Y.; Li, J.; Li, H. *Biosens. Bioelectron.,* 2022, **215**, 114569.

[6] Li, L.-L.; Liu, K.-P.; Yang, G.-H.; Wang, C.-M.; Zhang, J.-R.; Zhu, J.-J. *Adv. Funct. Mater.,* 2011, **21**, 869-878.

[7] Yang, L.; Jia, Y.; Wu, D.; Zhang, Y.; Ju, H.; Du, Y.; Ma, H.; Wei, Q. *Anal. Chem.,* 2019, **91**, 14066-14073.

[8] Su, X.; Wang, H.; Wang, C.; Zhou, X.; Zou, X.; Zhang, W. *Biosens. Bioelectron.,* 2022, **214**, 114546.

[9] Jia, B.; He, B.; Liu, R.; Yang, J.; Ren, W.; Suo, Z.; Xu, Y. *Food Chem.,* 2025, **470**, 142662.

[10] Wang, Q.; Yu, L.; Peng, Y.; Sheng, M.; Jin, Z.; Zhang, T.; Huang, J.; Yang, X. *Anal. Chem.,* 2024, **96**, 15624-15630.

[11] Zhao, D.-M.; Zhang, X.-H.; Feng, L.-J.; Jia, L.; Wang, S.-F. *Colloids Surf B Biointerfaces.,* 2009, **74**, 317-321.

[12] Li, J.; Liu, J.; Bi, Y.; Sun, M.; Bai, J.; Zhou, M. *Anal. Chim. Acta.,* 2020, **1105**, 87-94.

[13] Sha, H.; Zhang, Y.; Wang, Y.; Ke, H.; Xiong, X.; Xue, H.; Jia, N. *Biosens. Bioelectron.,* 2019, **132**, 203-209.

[14] Song, Z.; Miao, L.; Ruhlmann, L.; Lv, Y.; Li, L.; Gan, L.; Liu, M. *Angew. Chem. Int. Ed.,* 2023, **62**, e202219136.

[15] Y. Li, T. Yu, S. Peng, Q. Sun, D. Kong, C. Liu, Q. Zhang, Q. Shi, Y. Chen, *Microchem. J.*, 2024, **199**, 109929.

[16] Y. Li,·Q. Sun, X. Chen, S. Peng, D. Kong, C. Liu, Q. Zhang, Q. Shi,·Y. Chen, *Anal. Bioanal. Chem.*, 2024, **416**, 883-893.

[17] Y. Li, T. Yu, J. Li, D. Kong, Q. Shi, C. Liu, C. Dong, *Food Anal. Methods*, 2021, **14**, 2469-2477.

[18] S-K. Samaneh, M-A. Mohammad, R.K. Mohammad, E. Giti, H. Laleh, *Int. J. Food Prop.*, 2017, **20**, S119-S130.

[19] T. Yu, X. Chen, D. Sun, D. Kong, Z. Wang, F. Lin, Y. Li, *Food Biosci.*, 2024, **62**, 105565.